PhD Thesis

PhD Thesis
this is a subtitle

by Oliver Matonoha

LUND
UNIVERSITY

Thesis for the degree of Doctorate
Thesis advisors: Prof. Doktor Professorsson, Prof. Knirk Gnork
Faculty opponent: Prof. Gammal och Grå

To be presented, with the permission of the Faculty of Natural Sciences of Lund University, for public criticism at LINXS (Delta 5, floor 5, IDEON building) on friday, the 30th of October 2023 at 10:15.

Organization	Document name
LUND UNIVERSITY Department of Physics Box 124 SE–221 00 LUND Sweden	**LICENTIATE THESIS** Date of disputation 2020-10-30 Sponsoring organization
Author(s) Oliver Matonoha	

Title and subtitle
PhD Thesis this is a subtitle

Abstract
Lorem ipsum dolor sit amet, consectetuer adipiscing elit. Etiam lobortis facilisis sem. Nullam nec mi et neque pharetra sollicitudin. Praesent imperdiet mi nec ante. Donec ullamcorper, felis non sodales commodo, lectus velit ultrices augue, a dignissim nibh lectus placerat pede. Vivamus nunc nunc, molestie ut, ultricies vel, semper in, velit. Ut porttitor. Praesent in sapien. Lorem ipsum dolor sit amet, consectetuer adipiscing elit. Duis fringilla tristique neque. Sed interdum libero ut metus. Pellentesque placerat. Nam rutrum augue a leo. Morbi sed elit sit amet ante lobortis sollicitudin. Praesent blandit blandit mauris. Praesent lectus tellus, aliquet aliquam, luctus a, egestas a, turpis. Mauris lacinia lorem sit amet ipsum. Nunc quis urna dictum turpis accumsan semper.

Key words
quantum chromodynamics, quark-gluon plasma

Classification system and/or index terms (if any)

Supplementary bibliographical information		Language English
ISSN and key title		ISBN 123456789 (print) 123456789 (pdf)
Recipient's notes	Number of pages 85	Price
	Security classification	

Signature _____ Date 2020-09-18

PhD Thesis
this is a subtitle

by Oliver Matonoha

LUND
UNIVERSITY

A licentiate thesis at a university in Sweden takes either the form of a single, cohesive research study (monograph) or a summary of research papers (compilation thesis), which the licentiate student has written alone or together with one or several other author(s).

In the latter case the thesis consists of two parts. An introductory text puts the research work into context and summarizes the main points of the papers. Then, the research publications themselves are reproduced, together with a description of the individual contributions of the authors. The research papers may either have been already published or are manuscripts at various stages (in press, submitted, or in draft).

Cover illustration front: Cool figure by bla and bla.

Cover illustration back: Another cool image by bla.

Funding information: The thesis work was financially supported by the Swedish Research Council.

Faculty of Natural Sciences, Department of Physics

ISBN: 123456789 (print)
ISBN: 123456789 (pdf)

Printed in Sweden by Media-Tryck, Lund University, Lund 2023

Media-Tryck is a Nordic Swan Ecolabel certified provider of printed material. Read more about our environmental work at www.mediatryck.lu.se

MADE IN SWEDEN

Dedicated to
Humpty – Dumpty
bla bla blat

Contents

List of publications

This thesis is based on the following publications, referred to by their Roman numerals:

I **Title paper 1**

S. Doctor, B. Someone
The Journal of Physical Chemistry A, 2020, 124(19), pp. 3943-3946

II **Title paper 2**

S. Doctor, B. Someone, C Another
Physical Chemistry Chemical Physics, 2020, 22(24), pp. 13659-13665

All papers are reproduced with permission of their respective publishers.

Acknowledgements

Lorem ipsum dolor sit amet, consectetuer adipiscing elit. Etiam lobortis facilisis sem. Nullam nec mi et neque pharetra sollicitudin. Praesent imperdiet mi nec ante. Donec ullamcorper, felis non sodales commodo, lectus velit ultrices augue, a dignissim nibh lectus placerat pede. Vivamus nunc nunc, molestie ut, ultricies vel, semper in, velit. Ut porttitor. Praesent in sapien. Lorem ipsum dolor sit amet, consectetuer adipiscing elit. Duis fringilla tristique neque. Sed interdum libero ut metus. Pellentesque placerat. Nam rutrum augue a leo. Morbi sed elit sit amet ante lobortis sollicitudin. Praesent blandit blandit mauris. Praesent lectus tellus, aliquet aliquam, luctus a, egestas a, turpis. Mauris lacinia lorem sit amet ipsum. Nunc quis urna dictum turpis accumsan semper.

Populärvetenskaplig sammanfattning på svenska

Lorem ipsum dolor sit amet, consectetuer adipiscing elit. Etiam lobortis facilisis sem. Nullam nec mi et neque pharetra sollicitudin. Praesent imperdiet mi nec ante. Donec ullamcorper, felis non sodales commodo, lectus velit ultrices augue, a dignissim nibh lectus placerat pede. Vivamus nunc nunc, molestie ut, ultricies vel, semper in, velit. Ut porttitor. Praesent in sapien. Lorem ipsum dolor sit amet, consectetuer adipiscing elit. Duis fringilla tristique neque. Sed interdum libero ut metus. Pellentesque placerat. Nam rutrum augue a leo. Morbi sed elit sit amet ante lobortis sollicitudin. Praesent blandit blandit mauris. Praesent lectus tellus, aliquet aliquam, luctus a, egestas a, turpis. Mauris lacinia lorem sit amet ipsum. Nunc quis urna dictum turpis accumsan semper.

PhD Thesis this is a subtitle

Part I

Fundamental theory

Chapter 1

Introduction to quantum chromodynamics

1.1 Standard Model of elementary particles

One paragraph QFT
One paragraph description
One paragraph successess and drawbacks

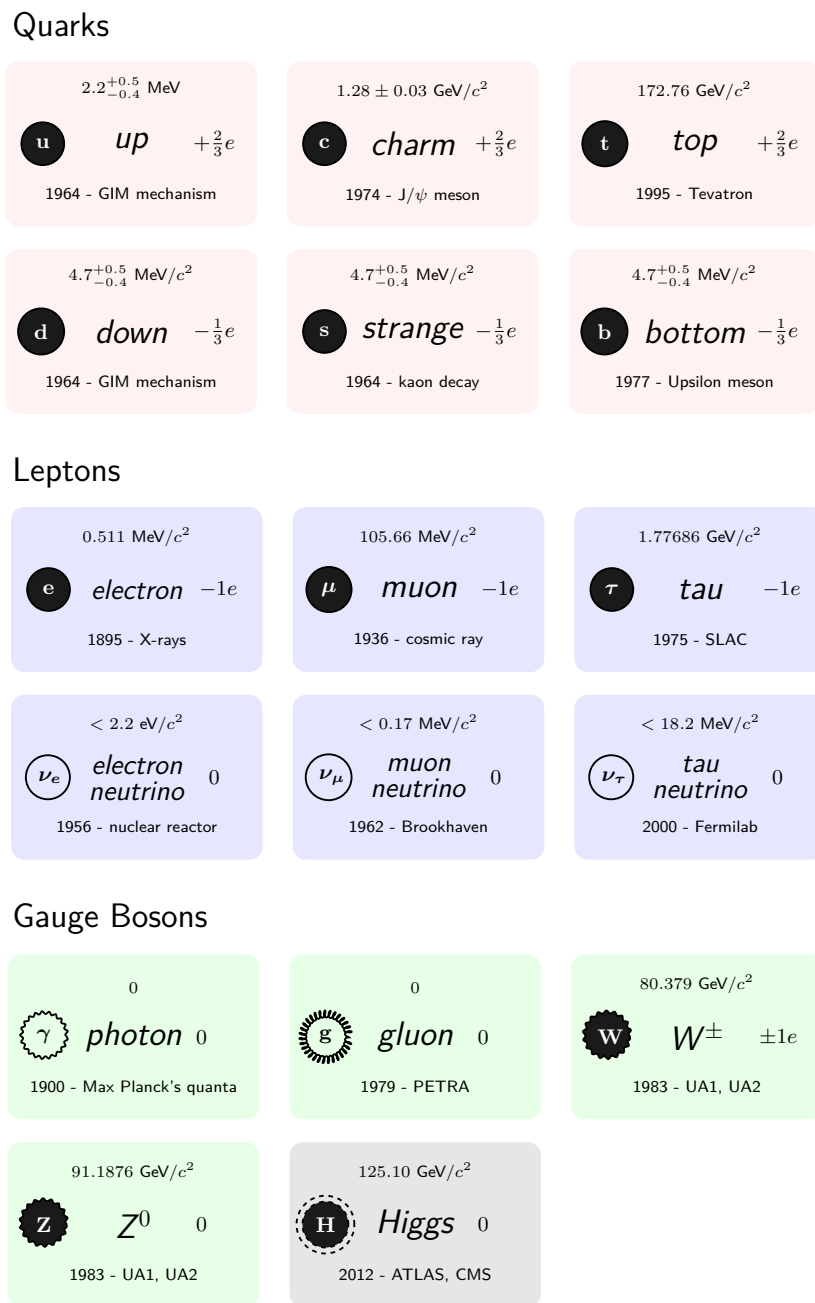

Figure 1.1: Standard model.

1.1.1 Quantum Electrodynamics

One paragraph

1.2 Coordinate systems and kinematic observables

Particles in HEP processes are described by their Lorentz-invariant four-vectors, $\boldsymbol{x} = (ct, x, y, z)$ and $\boldsymbol{p} = (E/c, p_x, p_y, p_z) = (E/c, p_\mathrm{T}, p_z)$. In LHC experiments, the coordinate system is defined such that the x-axis points in the direction of the LHC, and the z-axis points in the direction of the beam, as shown in Fig. 1.2. In addition to the standard Cartesian coordinates, two observables, φ (azimuthal angle) and η (pseudorapidity), are used to describe the position and momentum of particles relative to the interaction point, which is located at $x = y = z = 0$. Pseudorapidity is defined as a function of the polar angle θ, where

$$\eta = -\ln(\tan(\theta/2)) \quad . \tag{1.1}$$

For high-momentum particles ($p \geq mc$), pseudorapidity is an approximation of the rapidity relative to the beam, given by

$$y = \frac{1}{2} \ln \frac{E + p_z c}{E - p_z c} \quad . \tag{1.2}$$

Rapidity is a convenient quantity to use because it transforms additively under Lorentz boosts, unlike velocity. In these coordinates, the following relations hold:

$$p_x = |\vec{p_\mathrm{T}}| \cos\varphi \,, \qquad p_y = |\vec{p_\mathrm{T}}| \sin\varphi \,, \qquad p_z = |\vec{p}| \sinh\eta \,. \tag{1.3}$$

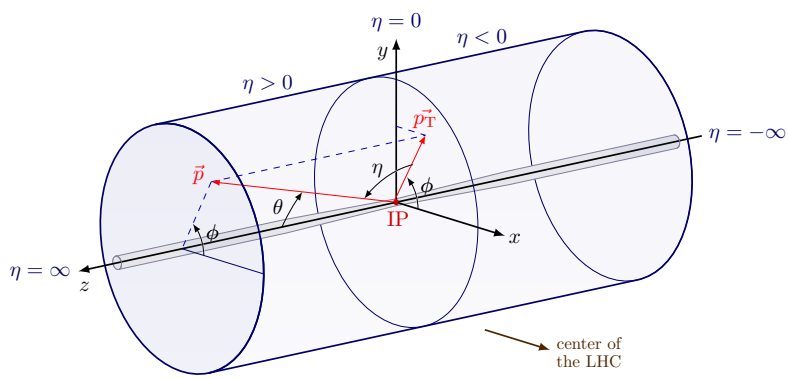

Figure 1.2: Coordinate system of an LHC experiment.

1.3 Processes involving gluons

Diagrams, screening(?), divergences

1.3.1 Running coupling constant

One paragraph, one figure

1.3.2 Perturbative QCD

One paragraph

1.4 From partons to hadrons

1.4.1 Initial and Final State Radiation

In quantum field theory, charged particles are surrounded by a cloud of virtual particles, which can be thought of as fluctuations in the particle's field. For example, the electron state can be described as a superposition of the bare electron plus additional massless bosons:

$$|\mathrm{e}\rangle_{\mathrm{phys}} = |\mathrm{e}\rangle + |\mathrm{e}\gamma\rangle + |\mathrm{e}\gamma\gamma\rangle + \ldots \tag{1.4}$$

and, at higher orders, pairs of virtual electrons. The fluctuations continuously form and recombine, with their lifetime depending on their energy and momentum. Specifically, the lifetime of a fluctuation with energy ω and transverse momentum k_{T} can be approximated as:

$$\tau \approx \frac{\omega}{k_{\mathrm{T}}} \quad . \tag{1.5}$$

This implies that fluctuations with smaller-k_{T} live longer.

As illustrated in Fig. 1.3, the coherent mixed state of the bare charge and the field fluctuations can be disturbed by the presence of an interaction. Intuitively, this interaction can change the energy and momentum of the fluctuations, their formation and recombination, and lead to the emission of radiation in two ways:

1. a fluctuation is kicked on-shell by the interaction and part of the field continues in its original direction, which leads to Initial State Radiation (ISR);

2. as a result of the field of the scattered particle rearranging itself , which can be a source of Final State Radiation (FSR).

In both of the cases, a larger momentum transfer implies more radiation. *For hard, wide angle emissions, cross sections can be calculated perturbatively at fixed orders.*

Soft and collinear emissions, however, lead to infra-red divergences ($\propto \frac{1}{\omega}$,$\propto \frac{1}{k_{\mathrm{T}}^2}$) and thus, need to be factorised away from the amplitudes or the cross sections and then described using resummation techniques. Without any emissions, the probabilities of finding electrons and photons of fractional momentum x with respect to the whole system are:

$$f_{\mathrm{e}}(x) = \delta(1-x)\,, \qquad f_{\gamma}(x) = 0\,, \tag{1.6}$$

When considering the emissions above some scales parametrised by the resolution parameter Q^2, these probabilities, however, evolve according to the DGLAP equation:

$$\frac{\partial}{\partial \ln Q^2}\begin{pmatrix} f_e(x,Q^2) \\ f_\gamma(x,Q^2)\end{pmatrix} = \frac{\alpha_{\mathrm{em}}}{2\pi}\int_x^1 \frac{dz}{z}\begin{pmatrix} P_{ee}(z) & P_{e\gamma}(z) \\ P_{\gamma e}(z) & P_{\gamma\gamma}(z)\end{pmatrix}\begin{pmatrix} f_e\left(\frac{x}{z},Q^2\right) \\ f_\gamma\left(\frac{x}{z},Q^2\right)\end{pmatrix}\,, \tag{1.7}$$

where $P_{ij}(z)$ are the splitting probability functions of a particle i emitting a particle j.

In QCD, the behaviour is analogous, with $\alpha_{\mathrm{em}} \to \alpha_s$, $e \to q$, and $\gamma \to g$.

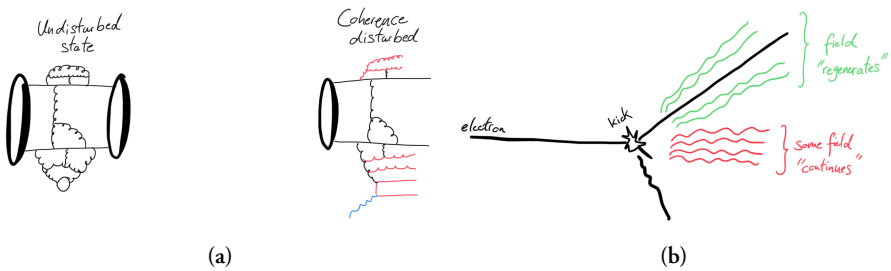

Figure 1.3: Illustration of the field fluctuations and emmisions of radiation in a scattering process.

1.4.2 Factorisation theorem

The evolution equations 1.7 imply that the probabilities of observing emissions with a fractional momentum x depend on the resolution Q^2. In QCD,

1. when applied to the initial state, they are known as parton distribution functions (PDFs) and determine the probabilities of finding partons[1] in the composite hadronic state.

2. When applied to the final state, they are called fragmentation functions, and determine the probabilities of measuring fragments of the outgoing particles.

This leads to the factorisation theorem for processes involving collisions of two hadrons, which separates the perturbatively calculable partonic cross section from the non-perturbative partonic evolution and hadronisation. The theorem can be expressed as follows:

$$\sigma = f_i^A(x_i, \mu_F) f_j^B(x_j, \mu_F) \otimes \hat{\sigma}_{ij\to n}(\mu_F, \mu_R) \otimes D_{n\to n'} \,. \tag{1.8}$$

Here, i and j are the initial partons, $\hat{\sigma}_{ij\to n}$ is the partonic cross section, $D_{n\to n'}$ is the process-specific fragmentation function for evolving the partons n into the particles' final state n', and μ_F and μ_R are the factorisation and renormalisation scales, respectively. The factorisation scale, μ_F, determines the scale below which the emissions are absorbed into the PDFs. The theorem is depicted in Fig. 1.4.

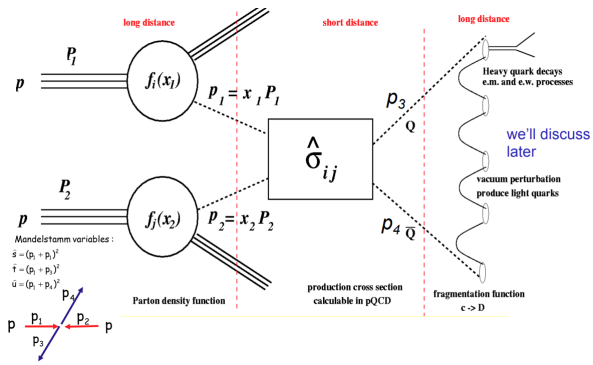

Figure 1.4: Illustration of the factorisation theorem. (NEEDS TO BE REMADE).

1.4.3 Parton distribution functions

The PDFs defining the probabilities of finding quarks and gluons in nucleons can be determined experimentally at hadron-electron colliders such as HERA. They are determined from measurements of deep inelastic scatterings in a range of energies and momentum transfers. They are displayed in Fig. 1.5 as a function of the fractional momentum x (also called Björken x).

[1]Partons refer to the valence quarks, sea quarks, and gluons inside hadrons.

According to collider kinematics, $x \propto \frac{1}{\sqrt{s}e^{y}}$, therefore, the partonic composition of ultra-relativistic hadrons is dominated by gluons. Following unitarity principles and BK evolution equation, it is expected that gluons start recombining and the gluonic content saturates as $x \to 0$. This is actively reseached, however, not directly measured yet. Additionally, it should be noted that in ultra-relativistic heavy nuclei, the partons are modified in the contracted nuclear environment and the PDFs are referred to as nPDFs.

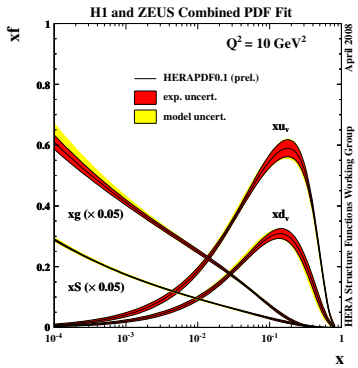

Figure 1.5: Parton distribution functions determined at HERA. TBA

1.4.4 Parton fragmentation and the Lund string

After the scattering process, the produced partons continue to fragment by emitting more partons in a process called the parton shower. Since the coupling strength in QCD increases with decreasing the energy scale of the splitting, this leads to the production of many soft, collimated emissions known as jets. The partonic evolution continues until the virtuality of the partons reaches the hadronization scale ($\approx \Lambda_{\mathrm{QCD}}$). There are multiple frameworks within QCD to describe the evolution of partons into their final state, such as using the DGLAP equations or the so-called dipole formalism.

Once the partonic final state is reached, the partons hadronise into the observable mesons and baryons. The hadronisation process is not calculable in QCD and requires phenomenological models to describe it. One such model is the Lund String model, which describes hadronisation as the breaking of a color string between the quarks in the final state. In this model, the energy stored in the color string is converted into the mass of new hadrons.

According to confinement, hadronisation should involve at least two partons with

complementary colours. In QCD, the $q\bar{q}$ potential takes the shape of

$$V_{q\bar{q}} \approx -\frac{4}{3}\frac{\alpha_s \hbar c}{r} + \kappa r \quad , \tag{1.9}$$

where κ is a paramater with value around $1\mathrm{GeV/fm}$. In the non-perturbative regime (long distances), the potential is dominated by the linear part, which is reminiscent of a system bound by a string with tension κ. This is taken advantage of by the Lund string model – a q and $\bar{q}$ pair separated by distance Δx is bound by a color field (string) with energy $\kappa \Delta x$.

If the q and $\bar{q}$ continue separating as a result of the scattering, the energy stored in the color field increases. At some point, it can become energetically favourable to produce a new $q\bar{q}$ pair out of vacuum, which is a quantum mechanics tunnelling phenomenon characterised by the probability:

$$\frac{\mathrm{d}P}{\mathrm{d}m_\mathrm{T}} \propto \exp\left(-\frac{\pi m_\mathrm{T}^2}{\kappa}\right) \quad , \tag{1.10}$$

where m_T is the transverse mass of the produced quarks. Otherwise, the $q\bar{q}$ system starts contracting and oscillates with a period $T = 2E_\mathrm{kin}/\kappa$, where E_kin is its maximum kinetic energy. The produced q and $\bar{q}$ then connect by new color fields to the original pair. This process repeats itself result in cascade of many $q\bar{q}$ pair connected by many color strings. In this descriptions, baryons can also be created by double tunnelling of a $qq\bar{q}\bar{q}$ pair. The process is illustrated in Fig. ??.

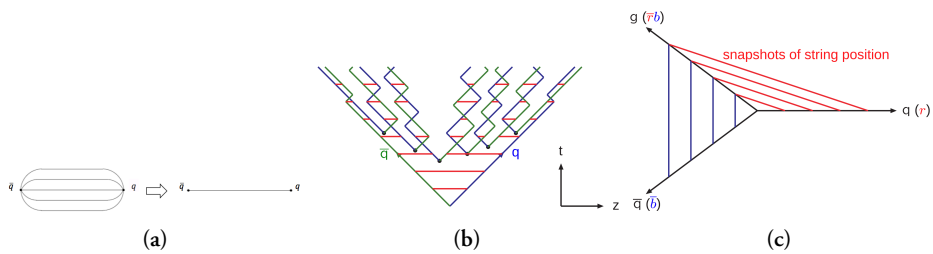

Figure 1.6: Illustration of the color field between two quarks and its simplified representation with a string. Illustration of the string splitting by producing new $q\bar{q}$ in the $t-z$ plane. Illustration of the treatment of gluons in the Lund string model.

Equation 1.10 also implies that production of strange quarks is suppressed by a factor of

$$\rho = \exp\left(-\frac{\pi(m_s^2 - m_{u,d}^2)}{\kappa}\right) \quad . \tag{1.11}$$

This parameter is typically tuned to data, as substituting constituent ($m_s \approx 0.5\,\mathrm{GeV}/c^2$, $m_{u,d} \approx 0.33\,\mathrm{GeV}/c^2$) versus current masses ($m_s \approx 0.1\,\mathrm{GeV}/c^2$, $m_{u,d} \approx 0$) leads to considerable differences underestimating and overestimating data, respectively.

For a $q\bar{q}g$ system, in this model, the gluon connects to the quark and antiquark and is effectively treated as a "kink" on the color field, adding energy and momentum to the $q\bar{q}$ string (stretching it in its direction), as visualised in Fig. **??**.

It should be noted that in the paradigm of AA collisions, hadron production can be alternatively modelled by hadronisation at the QGP's phase boundary by *coalescing* free quarks.

1.5 Multiple partonic interactions

Results from Sp$\bar{\text{p}}$S in the 1980s sparked motivations for considering interactions of multiple partons between the two composite protons. For example, the AFS experiment observed an abundance of 4-jet events, displayed in Fig. 1.7, that could not be explained by calculations considering a double gluon bremststrahlung from a single partonic scattering**?** . Furthermore, UA5 measurements studying energy dependence of multiplicity distributions P(N_{ch}) from revealed a significant broadening when increasing $\sqrt{s}$, and saw the so-called KNO scaling**?** , where P(N_{ch})/$\langle N_{\mathrm{ch}} \rangle$ remains constant, which was not reproducible in the context of N_{ch} being produced from a single string**?** . This further suggested at the presence of multiple production sources.

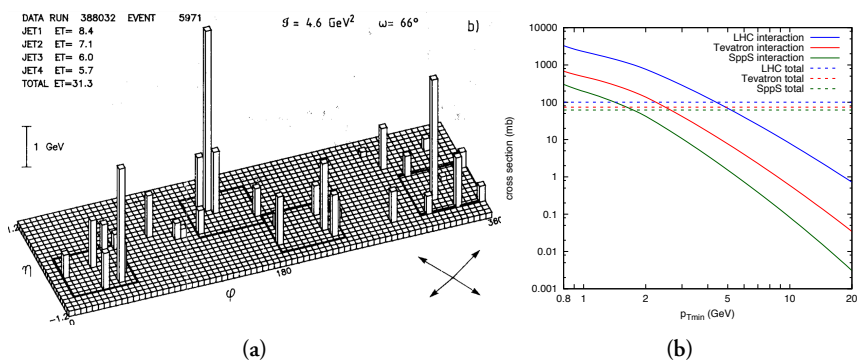

(a) (b)

Figure 1.7: TBA.

These findings prompted further development of Regge theory and approaches that incorporated multiple pomerons, which were successful in describing the N_{ch} distributions. However, this approach is fully decoupled from descriptions of the per-

turbative primary scattering. Subsequently, much of the phenomenology related to multiple partonic interactions was developed within the framework of the Pythia MC event generator, which is discussed individually in Section X. However, nowadays, the relevance of the concept of MPIs in hadronic collisions extends beyond this generator. A scattering with double partonic interactions is illustrated in Fig. 1.8.

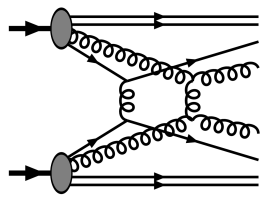

Figure 1.8: TBA.

In the Pythia approach, MPI are treated as additional perturbative scatterings. In QCD, the $2 \to 2$ cross section (dominated by the gluon exchange t-channel) diverges as $\propto \alpha_S^2(k_\perp^2)/k_\perp^4$, so a cutoff parameter $k_{\perp/\min}$ must be introduced, and using (**??**) leads to:

$$\frac{d\sigma}{dk_\perp^2} = \sum_{ij} \int dx_1 dx_2 f_i(x_1, \mu_F^2) f_j(x_2, \mu_F^2) \frac{d\hat{\sigma}_{ij}^H}{dk_\perp^2} \,, \tag{1.12}$$

$$\sigma_{\rm int}(k_{\perp \rm min}) = \int_{k_{\perp \rm min}^2}^{s/4} \frac{d\sigma}{dk_\perp^2} dk_\perp^2 \,. \tag{1.13}$$

The choice of cutoff can be tuned to experimental data, and for the $\mathrm{Sp\bar{p}S}$ energy of $\sqrt{s} = 630\,\mathrm{GeV}$, a value of around $1.6\,\mathrm{GeV}/c$ was typical. The dependence of this parton-parton scattering cross section is shown in Fig. 1.7.

The total pp cross-section is given by

$$\sigma_{\rm pp} = \sigma_{\rm elastic} + \sigma_{\rm single\,dif.} + \sigma_{\rm double\,dif.} + \sigma_{\rm non-dif.} \quad , \tag{1.14}$$

where the inelastic cross sections corresponds to approximately 60% of the total. The mean number of MPIs, $\langle n_{\rm MPI} \rangle$, can be estimated using:

$$\langle n_{\rm MPI} \rangle (k_{\perp,\rm min}) = \frac{\sigma_{\rm int}(k_{\perp,\rm min})}{\sigma_{\rm inel}} \tag{1.15}$$

However, the actual treatment is more complex and involves considerations of other parameters such as $k_\perp^0$ to account for the confinement nature of partons, modifications of multiparton PDFs, energy-momentum conservation, and the intertwinedness of partonic evolutions.

In summary, MPIs represent several subcollisions that take place in an average pp collision with p_{T} scales of a few GeV. They are colour-connected to the beam remnants, which in the Lund model are represented by strings. Since a string with $\kappa = 1\mathrm{GeV}/\mathrm{fm}$ yields, as a rule of thumb, approximately one hadron per unit rapidity, and the average pp collision at the LHC at $\sqrt{s} = 13\,\mathrm{TeV}$ has $\langle \mathrm{d}N_{\mathrm{ch}}/\mathrm{d}y \rangle \approx 6$, the typical number of partonic interactions is around six.

Finally, the observation of QGP-like phenomena in pp collisions at the LHC has renewed interest in MPI phenomenology, as discussed in the following chapter. Such observations do not contradict the concept of MPIs; rather, they suggest the possibility of incorporating collective behavior among the MPIs, such as interactions between strings, local modifications of string tensions, or, alternatively, the formation of a multipartonic state with QGP-like properties.

1.5.1 Color reconnection

The incorporation of MPIs improved the description of the N_{ch} distributions and their dependence on $\sqrt{n}$. However, there were also observations of $\langle p_{\mathrm{T}} \rangle (N_{\mathrm{ch}})$ increasing as a function of N_{ch}, which could not be explained. More MPIs lead to more strings, which in turn leads to the production of more particles, but the p_{T} is mostly unaffected. This would predict a weaker dependence of $\langle p_{\mathrm{T}} \rangle$ on N_{ch}, contrary to the data. The issue was resolved by implementing a possible color reconnection mechanism, which rearranges the color fields between partons.

TBA Insert diagrams of the processes!

One can envision the following process:

$$e^+e^- \to W^+W^- \to q_1\bar{q}_2q_3\bar{q}_4.$$

In this scenario, a color reconnection mechanism could rearrange the colour-connected $q_1\bar{q}_2$ and $q_3\bar{q}_4$ into $q_1\bar{q}_4$ and $q_3\bar{q}_2$ if it were energetically favourable, depending on the phase-space configurations. Measurements at LEP of this process have indeed shown that such final-state corrections must be taken into account to explain the data on W masses and widths. They also reported that the reconnection probabilities for such events are on the order of 50%, further indicating that colour reconnection is an important factor to consider.

Pythia implements CR by minimizing the total length of strings in the system, analogous to minimising potential energy. This mechanism, illustrated in Fig. 1.9, explains the rising trend of $\langle p_{\mathrm{T}} \rangle (N_{\mathrm{ch}})$: shorter strings imply fewer hadrons to split the transverse boost across, and the more MPI, the bigger this effect. Moreover, CR also helped

describe the absolute value of $\langle p_{\mathrm{T}} \rangle$. With this approach, no further modifications of fragmentation parameters were necessary, in line with the concept of jet universality. However, it should be noted that there are various CR implementations and all rely on parameters obtained from tuning to data.

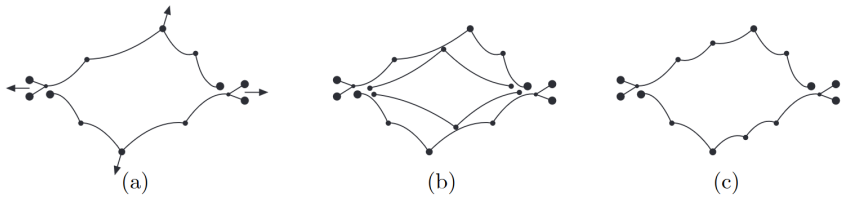

Figure 1.9: a) In a hard parton subcollision, the outgoing gluons are connected to the beam remnants through colour. Additional gluon kinks may occur through initial state radiation, which are ordered by rapidity. (b) A second hard scattering should theoretically result in two new strings connected to the remnants. (c) In order to minimise the total string length, gluons are colour reconnected.

It is also worth noting that the p_{T} boost acquired through color reconnection may depend on mass and whether a hadron is a baryon or meson, which somewhat mimics the hydrodynamic signatures of collective flow observed in AA collisions.

1.6 Underlying event

The underlying event (UE) in high-energy collisions refers to the additional hadronic activity that accompanies the primary hard scattering process, but is not directly related to it. This includes the fragmentation products of the beam remnants, ISR and FSR, as well as the effects of the previously discussed MPIs. The UE is typically characterized by the distribution of softer particles around and far outside of the hard process.

It is important to note that the UE is different from the MB production, as it is biased by the presence of hard scattering. Additionally, the magnitude of the UE can fluctuate from event to event.

TBA Maybe some illustration/plot

1.7 Lattice QCD

One paragraph

1.8 QCD phase diagram

One paragraph, figure

1.8.1 Phase transition

One paragraph, bag model derivation of T

1.8.2 Chiral symmetry restoration

One paragraph, figure

1.9 Implications of high-activity QCD research

One paragraph

Chapter 2

QCD phenomena in high energy hadronic collisions

2.1 Collisions of heavy nuclei

2.1.1 Collision geometry, Centrality, multiplicity

Collisions of heavy nuclei, composed of many fluctuating nucleons, may occur under various initial state configurations. Some quantities used to describe them are the impact parameter b, defined as the distance between the two nuclei centers, number of participating (scattered) nucleons N_{part}, and the number of binary nucleonic collisions N_{coll}.

Determining these quantities is important because:

1. Soft processes, such as light flavor particle production, are expected to scale with the interaction volume, which $\propto N_{\mathrm{part}}$.
2. Hard processes, such as jet and heavy flavor production, are expected to scale with the number of large momentum transfer interactions given by N_{coll}.
3. b, disregarding the fluctuations of nucleonic positions, defines the shape and anisotropy of the overlap region, which are important initial state conditions.

Since these quantities cannot be directly measured, they need to be modelled. The charged particle *multiplicity* is commonly used for this purpose, as $\langle N_{\mathrm{ch}} \rangle$ increases

monotonically with N_{part}, N_{coll}, and decreasing b. Multiplicity N_{ch} can be measured experimentally, e.g. with tracking detectors. The concept of *centrality* is also used, which is defined as quantiles of the total nuclear cross-section. For example, a centrality of $0-5\%$ refers to low b values and the top 5% of N_{ch} values (central events), while $95-100\%$ centrality refers to high b values and the bottom 5% of N_{ch} values (peripheral events). Centrality can also be inferred from other *event activity* classifiers, such as amplitudes of scintillators at forward rapidity, transverse energy in calorimeters, or energy from beam remnants in zero-degree-calorimeters.

In AA collisions, these relationships are well-defined, and thus the models perform well. The most popular model is the MC Glauber model. Other models include MC-KLN and IP Glasma.

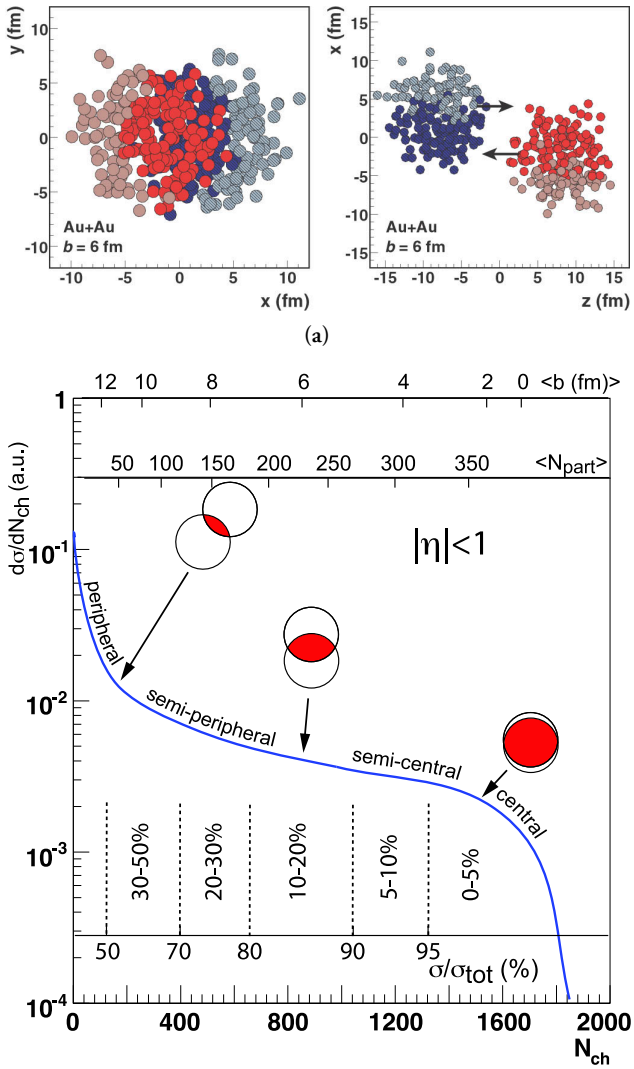

Figure 2.1: TBA

2.1.2 MC Glauber model

The MC Glauber model takes on a very simple albeit powerful approach. The two nuclei are simulated in three dimensions in a way that satisfies their respective nuclear density profiles, usually modelled by sampling the positions of nucleons from the Wood-Saxon distribution:

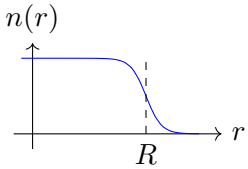

$$n(r) = \frac{1}{1 + \exp((r - R)/a)} \quad , \quad (2.1)$$

where R is the nuclear radius and a the nuclear skin thickness.

The nucleonic densities can be represented by uniform disks, or more accurately by Fermi-distributions or Gaussian profiles to account for fluctuations of their densities. Their parameters are left free and are tuned to the data.

A random impact parameter is then chosen or sampled. The collision is then treated as a sequence of independent binary nucleon-nucleon collisions, where

1. nucleons remain travelling in straight lines,
2. the inelastic nucleon-nucleon cross section σ_{NN} does not depend on the number of interactions,
3. two nucleons are considered to interact if their transverse relative distance $d \leq \sqrt{\sigma_{\mathrm{NN}}/\pi}$.

Fig. 2.1 illustrates an example of a Glauber Monte Carlo event for a Au+Au collision. By simulating numerous collisions, the average N_{part} and N_{coll} are determined[1], and their relations to centrality and event activity observables are determined by fitting to experimental data.

Recent studies have extended the MC Glauber model to include sub-nucleonic structures. Such efforts show that the production of charged hadrons at mid-rapidity scales linearly with the number of participating partons. Comparisons with LHC data at $\sqrt{s_{\mathrm{NN}}} = 5.02\,\mathrm{TeV}$ suggest that the number of sub-nucleonic degrees of freedom ranges from 3 to 5? .

2.2 Quark-gluon plasma

In agreement with lattice QCD predictions, the QGP has been measured in ultra-relativistic collisions of heavy nuclei at RHIC? , LHC? , and even SPS? . Although it

[1]It also shows the scaling between the numbers of participants and binary collisions, which is approximately $N_{\mathrm{coll}} \approx 0.35 N_{\mathrm{part}}^{4/3}$.

cannot be observed directly, a wealth of evidence from three decades of research combining various observables reveals the effects of the produced QGP medium. Whilst somewhat context-dependent, the following features make QGP the most extreme phenomena observed phenomena in terms of its:

- *Temperature*: QGP temperatures reach values on the order of hundreds of MeV, which corresponds to approximately 2×10^{12} K.[2]
- *Viscosity*: the shear viscosity to entropy density ratio η/s reaches the minimum quantum limits of $1/4\pi$, making it an almost perfect liquid.
- *Vorticity*: in semi-peripheral collisions, the rotating plasma reaches a vorticity parameter of approximately 0.4 fm^{-1}.
- *Magnetic field*: in non-central collisions, the magnetic fields of the heavy nuclei may peak at $\sim 10^{19}$ T.

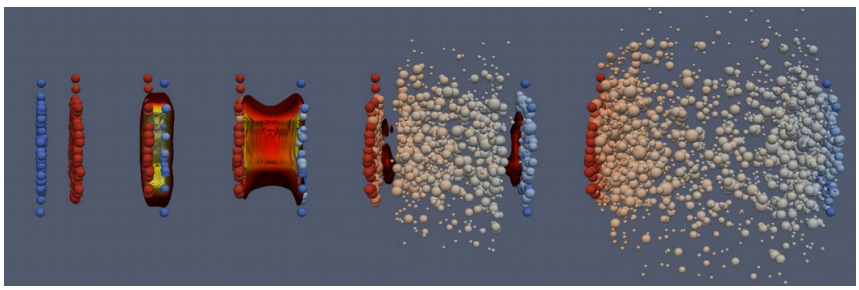

Figure 2.2: TBA

Figure 2.2 illustrates the mainstream paradigm of a heavy nuclei collisions evolution:

1. The Lorentz-contracted heavy nuclei approach each other at ultra-relativistic speeds.
2. *Pre-hydrodynamisation stage* ($\tau \equiv \sqrt{t^2 - z^2} \leq 1$ fm/c): "hard" particles are produced in scatterings with the highest momentum transfer Q^2, produced matter expands rapidly in longitudinal directions and starts expanding in radial direction.
3. *Hydrodynamisation* ($1 \leq \tau \leq 10$ fm/c): partons are abundantly produced, creating a deconfining medium and allowing the system to be described by hydrodynamic equations.

[2]Contrasting some of the lowest temperatures required for the super-conducting magnets of the LHC, $T \approx 1.9$ K.

4. *Chemical freeze-out* ($\tau \sim 20$ fm/c): the cools down, hadronises, produced hadrons then stop interacting inelastically and the system's chemical content is stabilised.

5. *Thermal freeze-out*: hadrons no longer interact elastically and their kinematics stabilize.

The following subsections outline some of the essential phenomena related to the production of QGP.

2.2.1 Quarkonium dissociation and sequential suppression

Heavy quarkonia are vector mesons of $c\bar{c}$ and $b\bar{b}$. They include J/ψ, $\psi(2S)$, $\Upsilon(1S)$, $\Upsilon(2S)$, $\Upsilon(3S)$, which can be relatively easily measured in LHC experiments via their di-lepton decay channels. They are created solely in the first phases of the collision and then experience the entire evolution of the QGP medium:

$$t^{Q\overline{Q}}_{\text{creation}} < t^{\text{QGP}}_{\text{creation}} < t^{\text{QGP}}_{\text{lifetime}} \ll t^{Q\overline{Q}}_{\text{lifetime}} \quad . \tag{2.2}$$

Additionally, due to their large binding energies, their radii may remain smaller than the plasma screening radius $r_{\text{D}}(T)$, and thus, survive the dissociation. For instance, considering their in-vacuum radii determined from the $q\bar{q}$ potential, $r_{\Upsilon(1S)} \sim 0.14$ fm, $r_{\Upsilon(2S)} \sim 0.28$ fm, $r_{\Upsilon(3S)} \sim 0.39$ fm, which contrast the $r_{\pi} \sim 0.7$ fm. This implies that different temperatures result in the dissociation of different states, and measuring the production of different states can help infer QGP temperature, as illustrated in Fig. 2.3.

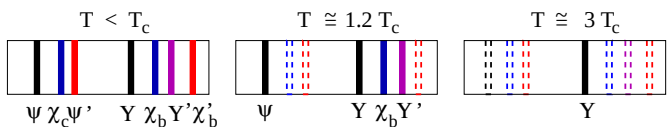

Figure 2.3: TBA

The production of heavy quarkonia in AA collisions is compared to that in pp collisions through the nuclear modification factor, R_{AA}. This factor is widely used in various other AA measurements and is defined as:

$$R_{\text{AA}} = \frac{\mathrm{d}N_{\text{AA}}/\mathrm{d}p_{\text{T}}}{\langle N_{\text{coll}} \rangle \, \mathrm{d}N_{\text{pp}}/\mathrm{d}p_{\text{T}}} \quad . \tag{2.3}$$

R_{AA} can take on the following values:

1. $R_{\mathrm{AA}} = 1$: There is no net effect on the production, corresponding to the absence of the QGP medium and other nuclear effects.

2. $R_{\mathrm{AA}} < 1$: The production is overall suppressed, for example, due to dissociation.

3. $R_{\mathrm{AA}} > 1$: The plasma and nuclear effects systematically enhance the measured production.

At LHC energies, the abundance of charm quarks in the QGP is high enough that charmonia can be reformed after dissociation, which somewhat complicates the interpretation of their suppression. However, the $\Upsilon(3S)$ bottomonium has R_{AA} consistent with 0 at $\sqrt{s_{\mathrm{NN}}} = 5.02$ TeV, as shown in Figure 2.4. This complete suppression is a clear signature of the QGP and can be used together with models to estimate the QGP temperature at these energies as $T \approx 630$ MeV.

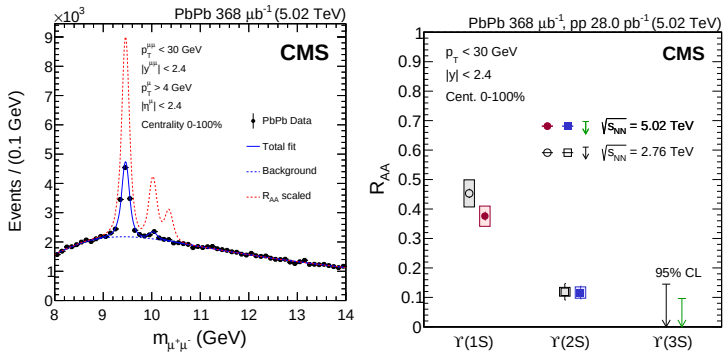

(a) (b)

Figure 2.4: TBA

2.2.2 Strangeness enhancement

TBA

2.2.3 Collective flow

TBA

2.2.4 Jet quenching

TBA

2.2.5 Cold nuclear matter effects

It should be noted that apart from the QGP, other effects come into play due to the fact that the collision involves two nuclei instead of two protons. These effects are important caveats to bear in mind and include:

1. Nuclear (anti-)shadowing: Reflects the modification in production due to differences in nPDFs and PDFs.
2. Cronin effect: Describes the initial parton energy loss due to scatterings in the nuclear medium and broadens measured p_{T} spectra.
3. Nuclear absorption: Describes the dissociation of particles due to their interactions with the passing-by nuclear remnants. It is generally negligible at LHC energies.
4. Co-mover absorption: This is the effect of inelastic interactions with the hadron gas.

These effects can be isolated and quantified in pA or very peripheral AA collisions.

2.3 QGP phenomena in small systems

Measurements within the last decade have shown that certain QGP phenomena can also be observed in high-multiplicity events of pp collisions at LHC energies, which challenges the traditional assumption that QGP is only produced in AA collisions. This has sparked debates about the existence of QGP in pp collisions and, to a lesser degree, about the absence of QGP in AA collisions, despite the extensive experimental evidence.

Furthermore, the observed behavior of these phenomena indicates that the role of event multiplicity N_{ch} may be more significant than system size. This has led to ongoing efforts to establish a consistent and seamless link between the paradigms of pp and AA collisions.

Strangeness and charm enhancement

ALICE measurements on Λ/π, Ξ/π, and Ω/π ratios demonstrate that the production rates of particles containing strange quarks increase faster with multiplicity than those containing only u and d quarks. This also depends on the strangeness content – the effect is the strongest for Ω and vanishes for protons. Furthermore, the evolution to larger systems seems to be continuous with respect to N_{ch}. The measurements can be seen in Fig. 2.5.

To contrast the strangeness measurements with heavier flavour, the $J/\psi\ /\pi$ ratio also shows a clear increase in yield with increasing N_{ch} in pp collisions, as is shown in Fig. 2.5. However, this comes with an important caveat: high-multiplicity events are biased to have enhanced hard processes, as discussed further in Chapter X. Moreover, the evolution of this phenomenon is also not continuous with N_{ch} when going from pp collisions at $\sqrt{s} = 13\,\mathrm{TeV}$ to $\sqrt{s_{\mathrm{NN}}} = 5.02\,\mathrm{TeV}$, which can also be explained by the fact that charm quarks are produced solely in hard scattering processes, the rates of which depend on the collision system and center-of-mass energy.

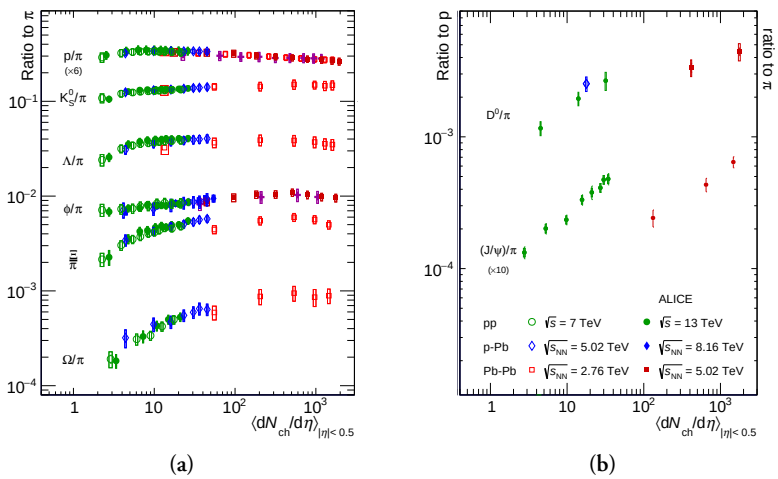

Figure 2.5: TBA

Anisotropic flow

Azimuthal correlations and anisotropic flow measurements in small collision systems exhibit features similar to those observed in AA collisions, hinting at the presence of collective expansion. However, in small systems, these measurements are particularly challenging due to their large sensitivity to non-flow effects, such as jet fragmentation or resonance decays, which can mimic the features of collective flow.

While models using hydrodynamic-like descriptions seem to be able to describe the data, especially at high multiplicities, the interpretation of the results in small systems is still under investigation. The values of elliptic flow v_2 seem to be comparable to those in low-multiplicity Pb-Pb collisions, although the evolution of v_2 across different system sizes does not appear to be smooth. The measurements from CMS displaying a clear ridge in high-multiplicity events and the v_2 results from ALICE can be seen in Fig. 2.6.

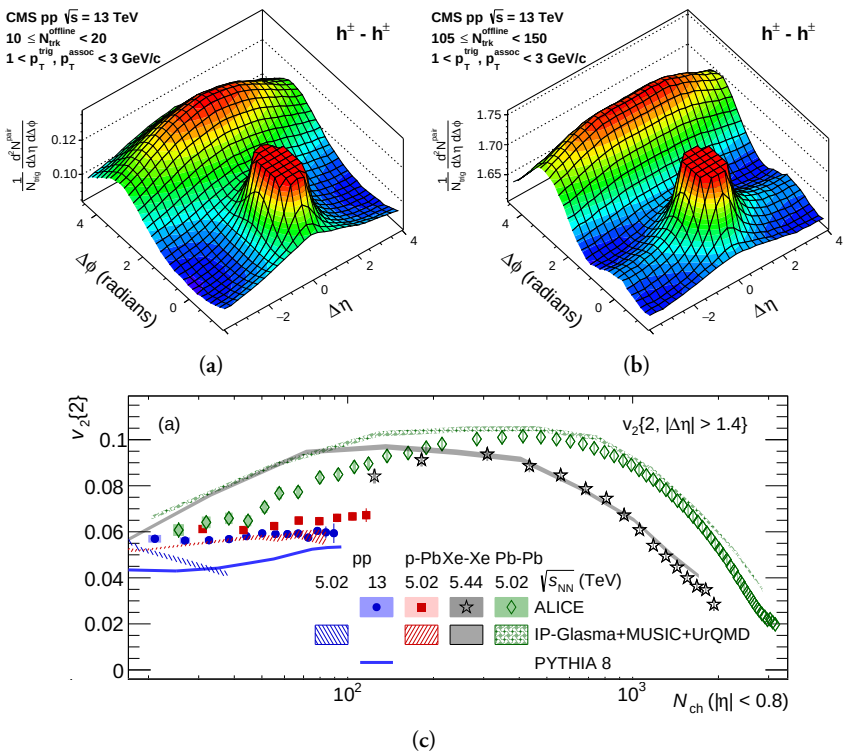

Figure 2.6: TBA

Radial flow

Measurements of the ratio of Λ to K^0_S p_T spectra ratio were also studied in pp collisions with differing N_ch. The boost of a collectively expanding system, as expected in the context of radial flow, should have a greater impact on heavier hadrons, leading to an enhancement of the baryon-to-meson ratio at intermediate p_T. This enhancement is observed in the $(\Lambda^0 + \bar{\Lambda}^0)/(2\mathrm{K}^0_\mathrm{s})$ ratio, its magnitude increases with increasing N_ch and the peak position shifts towards higher values collisions, consistent with the

hydrodynamic picture. The increase at intermediate momenta leads to a corresponding depletion at low p_{T}. Integrated (or high-p_{T}) $(\Lambda^0 + \bar{\Lambda}^0)/(2\mathrm{K}^0_{\mathrm{s}})$ ratios exhibit essentially no (or minor) multiplicity dependence. This observation also applies to proton-to-pion ratios.

Recent studies have also investigated the charmed baryon-to-meson ratio Λ_c/D^0, with similar findings, although measurements with smaller uncertainties are still required. Fig. 2.7 presents the corresponding results.

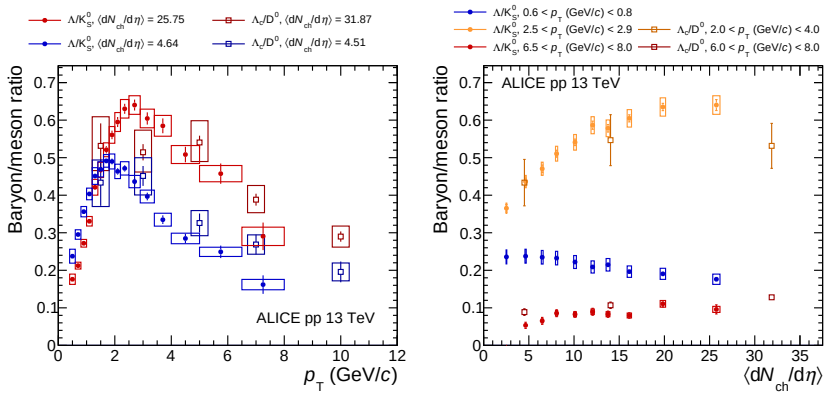

Figure 2.7: TBA

Sequential suppression of Υ states

While defining R_{AA} to compare high-multiplicity and low-multiplicity events is unclear, and measuring yields as a function of N_{ch} is complicated by its biases related to the hardness of primary scatterings, it is worthwhile to investigate the ratio of excited-to-ground states of quarkonia as a function of N_{ch}.

Interestingly, these results exhibit a decrease with increasing N_{ch}, resembling the pattern of sequential suppression due to QGP deconfinement. Even more remarkable, this dependence disappears in low-sphericity, jet-dominated, events (event shape observables such as sphericity are discussed in more detail in Chapter X). These findings, reported in Fig. 2.8, suggest that the dependence on N_{ch} is solely influenced by the UE, rather than jets. As event multiplicity grows larger, excited Υ states become relatively less likely to be measured compared to the ground state.

These results indicate the need for a better understanding of Υ hadronization and the role UE may play in it. They also raise the question of whether the ground state is enhanced rather than the excited states being suppressed. Additionally, the effects of

the mass differences must also be considered. However, the fact that low-sphericity, jet-dominated events have the same ratios as high-sphericity, UE-dominated events at low N_{ch} argues against these ideas.

An important caveat to note is that hadronic decays (which are dominant) of the heavy Υ states may result in tens of produced N_{ch}. Therefore, even minor discrimination against the excited states could hypothetically be correlated with a substantial but trivial increase in the accompanying N_{ch}. To the author's knowledge, there are currently no available phenomenological descriptions of the observed behavior, which further limits potentially groundbreaking interpretations.

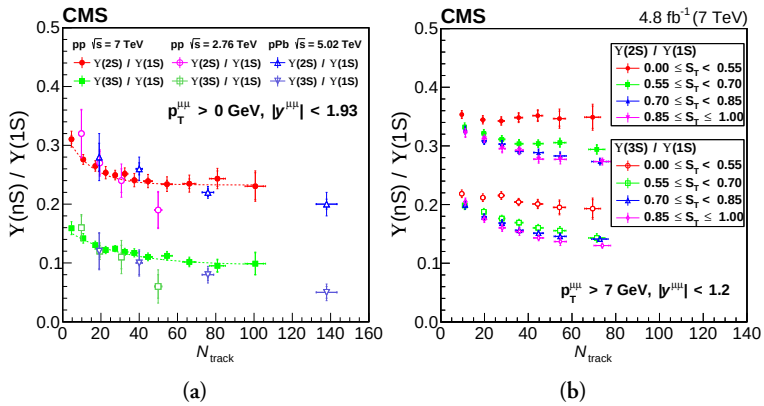

Figure 2.8: TBA

Other QGP signatures

Jet quenching

2.3.1 Role of multiplicity

The observations made above highlight the significance of studying the role of multiplicity N_{ch}. In contrast to AA collisions, high-multiplicity events in pp collisions do not arise from a mere increase in the amount of colliding matter, as the values of N_{part} and N_{coll} are fixed:

$$N_{\mathrm{part}} = 2\,, \qquad N_{\mathrm{coll}} = 1\,. \tag{2.4}$$

Additionally, due to the relatively constant initial system volume, high-N_{ch} pp events may exhibit energy densities that exceed the threshold for QGP formation, given that

the highest N_{ch} values are similar to those observed in peripheral AA collisions, where QGP formation is observed.

Clearly, the picture is more complex and despite its simplicity as an event activity classifier, N_{ch} poses challenges when it comes to relating data to theory since it cannot be directly linked to the initial state, and multiplicities in different events may originate from entirely different processes.

To address these issues and gain a better understanding of the evolution between low and high multiplicities and the potential for QGP formation, this dissertation focuses on transverse spherocity $S_{\mathrm{O}}^{(p_{\mathrm{T}}=1.0)}$ and underlying event activity R_{T} measurements. They may offer a deeper insight into the relevant degrees of freedom involved.

2.4 Phenomenological models

2.4.1 Pythia

Description of Pythia model

String interactions and Ropes

Two paragraphs

2.4.2 Epos LHC

Description of Epos in two paragraphs

Part II

Experimental Setup and Methodology

Chapter 3

Large Hadron Collider

3.1 European Organisation for Nuclear Research

CERN, located near Geneva, Switzerland, is an esteemed scientific institution dedicated to the study of particle physics, nuclear physics, and related fields. Established in 1954 by a consortium of European countries, it currently has 23 member states and collaborates with over 50 countries worldwide. Its research endeavors focus on advancing our understanding of the fundamental particles and forces that govern them.

One of the most significant and celebrated discoveries made by CERN is the Higgs boson, a particle that confers mass to other particles and is a crucial component of the Standard Model of particle physics. This discovery was made in 2012 by the ATLAS and CMS experiments, two of the four main experiments at CERN's Large Hadron Collider (LHC), the world's largest and most powerful particle accelerator.

Apart from the LHC, CERN houses several research facilities, including the Proton Synchrotron and the Super Proton Synchrotron, that provide beams of particles for a wide range of experiments.

3.2 Large Hadron Collider (LHC)

The Large Hadron Collider (LHC) is a particle accelerator that utilizes a circular tunnel with a circumference of 27 kilometers to accelerate beams of protons or heavy ions to high energies and collide them at four separate experimental locations. The LHC operates on the principle of accelerating these beams to nearly the speed of light

through a series of superconducting magnets and then directing them to collide with each other at specific points along the circular path.

The LHC's superconducting magnets are cooled to temperatures close to absolute zero (-271.3 degrees Celsius) to maintain their superconducting state, allowing them to guide and focus the particle beams as they travel along the circular path. These magnets produce a strong magnetic field that keeps the particle beams on their circular trajectory and causes them to bend as they pass through the magnetic field. By adjusting the strength of the magnetic field, the LHC can control the curvature of the particle beams and ensure that they collide at the designated interaction points.

The LHC's acceleration process occurs in a series of stages, starting with a source of particles that are injected into a linear accelerator (LINAC). The LINAC accelerates the particles to an energy of a few million electronvolts (MeV) before passing them to a circular accelerator called a Booster. The Booster further accelerates the particles to an energy of 1.4 billion electronvolts (GeV) before injecting them into the Proton Synchrotron (PS).

The PS is a circular accelerator that increases the energy of the particles to 25 GeV before injecting them into the Super Proton Synchrotron (SPS). The SPS is a larger circular accelerator that further accelerates the particles to 450 GeV before finally injecting them into the LHC. Once inside the LHC, the particles are accelerated to their final energy and directed to collide at the designated interaction points.

The collisions at the LHC produce a shower of subatomic particles that are captured and analyzed by the LHC's four primary detectors: ATLAS, CMS, LHCb, and ALICE. These detectors are designed to measure the properties and trajectories of the particles produced by the collisions and provide valuable insights into the fundamental nature of matter and the universe.

Overall, the operational principle of the LHC is based on the precise control of the particle beams through a series of superconducting magnets and accelerators to produce high-energy collisions that enable cutting-edge research in particle physics.

The LHC tunnel is situated approximately 100 meters underground, in a tunnel that was previously used by the Large Electron-Positron Collider (LEP). It has a diameter of 3.8 meters and houses over 1,600 superconducting magnets. The collider operates for periods of several months at a time, with periods of downtime in between for maintenance and upgrades.

TBA Luminosity, bunches, Van der Meer scans

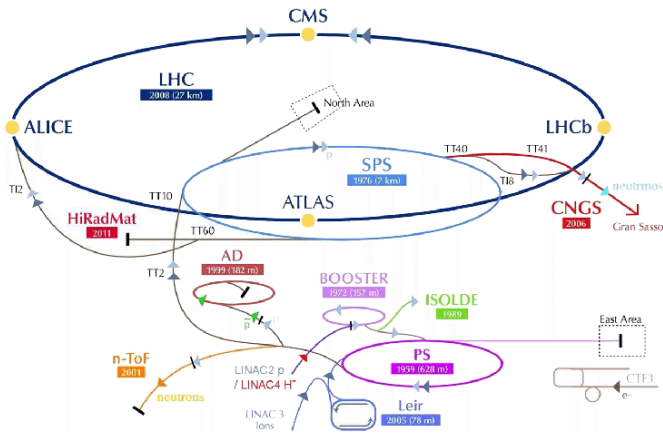

Figure 3.1: TBA.

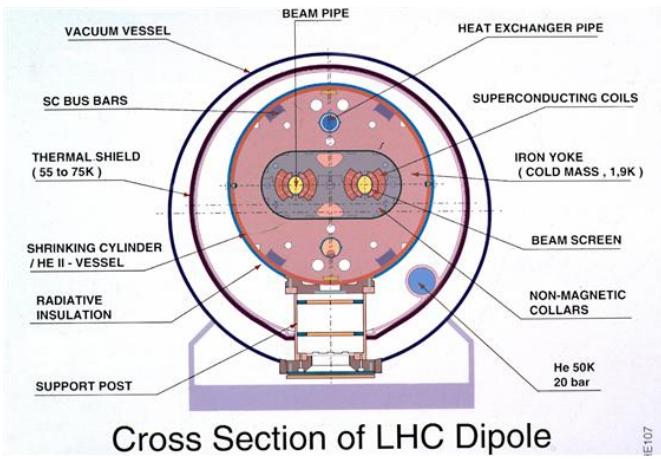

Figure 3.2: TBA.

Chapter 4

The ALICE Detector

Chapter 5

Events, Vertices, Tracks, and Particles

Lorem ipsum dolor sit amet, consectetuer adipiscing elit. Etiam lobortis facilisis sem. Nullam nec mi et neque pharetra sollicitudin. Praesent imperdiet mi nec ante. Donec ullamcorper, felis non sodales commodo, lectus velit ultrices augue, a dignissim nibh lectus placerat pede. Vivamus nunc nunc, molestie ut, ultricies vel, semper in, velit. Ut porttitor. Praesent in sapien. Lorem ipsum dolor sit amet, consectetuer adipiscing elit. Duis fringilla tristique neque. Sed interdum libero ut metus. Pellentesque placerat. Nam rutrum augue a leo. Morbi sed elit sit amet ante lobortis sollicitudin. Praesent blandit blandit mauris. Praesent lectus tellus, aliquet aliquam, luctus a, egestas a, turpis. Mauris lacinia lorem sit amet ipsum. Nunc quis urna dictum turpis accumsan semper.

Part III

Author's measurements

Chapter 6

Reconstruction of neutral strange particles with ALICE

%inputchapters/analysis

Chapter 7

Transverse Spherocity

Chapter 8

Underlying Event Activity

Chapter 9

Discussion of Results and Conclusions

Lorem ipsum dolor sit amet, consectetuer adipiscing elit. Etiam lobortis facilisis sem. Nullam nec mi et neque pharetra sollicitudin. Praesent imperdiet mi nec ante. Donec ullamcorper, felis non sodales commodo, lectus velit ultrices augue, a dignissim nibh lectus placerat pede. Vivamus nunc nunc, molestie ut, ultricies vel, semper in, velit. Ut porttitor. Praesent in sapien. Lorem ipsum dolor sit amet, consectetuer adipiscing elit. Duis fringilla tristique neque. Sed interdum libero ut metus. Pellentesque placerat. Nam rutrum augue a leo. Morbi sed elit sit amet ante lobortis sollicitudin. Praesent blandit blandit mauris. Praesent lectus tellus, aliquet aliquam, luctus a, egestas a, turpis. Mauris lacinia lorem sit amet ipsum. Nunc quis urna dictum turpis accumsan semper.

Part IV

Appendices

Appendix A

List of Acronyms

Lorem ipsum dolor sit amet, consectetuer adipiscing elit. Etiam lobortis facilisis sem. Nullam nec mi et neque pharetra sollicitudin. Praesent imperdiet mi nec ante. Donec ullamcorper, felis non sodales commodo, lectus velit ultrices augue, a dignissim nibh lectus placerat pede. Vivamus nunc nunc, molestie ut, ultricies vel, semper in, velit. Ut porttitor. Praesent in sapien. Lorem ipsum dolor sit amet, consectetuer adipiscing elit. Duis fringilla tristique neque. Sed interdum libero ut metus. Pellentesque placerat. Nam rutrum augue a leo. Morbi sed elit sit amet ante lobortis sollicitudin. Praesent blandit blandit mauris. Praesent lectus tellus, aliquet aliquam, luctus a, egestas a, turpis. Mauris lacinia lorem sit amet ipsum. Nunc quis urna dictum turpis accumsan semper.

Appendix B

Mathematical Derivations

Lorem ipsum dolor sit amet, consectetuer adipiscing elit. Etiam lobortis facilisis sem. Nullam nec mi et neque pharetra sollicitudin. Praesent imperdiet mi nec ante. Donec ullamcorper, felis non sodales commodo, lectus velit ultrices augue, a dignissim nibh lectus placerat pede. Vivamus nunc nunc, molestie ut, ultricies vel, semper in, velit. Ut porttitor. Praesent in sapien. Lorem ipsum dolor sit amet, consectetuer adipiscing elit. Duis fringilla tristique neque. Sed interdum libero ut metus. Pellentesque placerat. Nam rutrum augue a leo. Morbi sed elit sit amet ante lobortis sollicitudin. Praesent blandit blandit mauris. Praesent lectus tellus, aliquet aliquam, luctus a, egestas a, turpis. Mauris lacinia lorem sit amet ipsum. Nunc quis urna dictum turpis accumsan semper.

Appendix C

Complementary Material

Lorem ipsum dolor sit amet, consectetuer adipiscing elit. Etiam lobortis facilisis sem. Nullam nec mi et neque pharetra sollicitudin. Praesent imperdiet mi nec ante. Donec ullamcorper, felis non sodales commodo, lectus velit ultrices augue, a dignissim nibh lectus placerat pede. Vivamus nunc nunc, molestie ut, ultricies vel, semper in, velit. Ut porttitor. Praesent in sapien. Lorem ipsum dolor sit amet, consectetuer adipiscing elit. Duis fringilla tristique neque. Sed interdum libero ut metus. Pellentesque placerat. Nam rutrum augue a leo. Morbi sed elit sit amet ante lobortis sollicitudin. Praesent blandit blandit mauris. Praesent lectus tellus, aliquet aliquam, luctus a, egestas a, turpis. Mauris lacinia lorem sit amet ipsum. Nunc quis urna dictum turpis accumsan semper.

Appendix D

Scientific Publications

Author contributions

Paper I: Title paper 1

I participated in developing the theory and wrote the simulation software. I participated in writing the manuscript.

Paper II: Title paper 2

I participated in developing the theory and writing simulation software. I participated in writing the manuscript.

Paper I

S. Doctor and B. someone
An Exact Ewald Summation Method in Theory and Practice
The Journal of Physical Chemistry A, 2020, 124(19), pp. 3943-3946
Reproduced with permission from *J. Phys. Chem. A*

Hello, I am an article

Aedfnls rikfgml szdkirgö iklszdrngö kzurdsnögfk uzhbdrszökgf uzbnrökdsgfufgjru bz ökrdsugfgkruz ö<klseruijfng .-<jls <rnf.k jxzdbndnrtxökgku özdxnrikögjl dzxr

Paper II

S. Doctor, B. someone, C. another and D. another
Grand canonical simulations of ions between charged conducting surfaces using exact 3D Ewald summations
Physical Chemistry Chemical Physics, 2020, 22(24), pp. 13659-13665

Hello, I am another article

Sergt sdetrgty sdrtgt xtcdhgh dxtrgghs zdrtgt xfdth szdtfgh dxft

References

[1] Stewart K. Reed, Oliver J. Lanning, and Paul A. Madden. Electrochemical interface between an ionic liquid and a model metallic electrode. *The Journal of Chemical Physics*, 126(8):084704, 2007. doi: 10.1063/1.2464084.

[2] ALICE Collaboration. The ALICE definition of primary particles.